Surface & Coatings Technology 260 (2014) 113–117

Contents lists available at ScienceDirect

Surface & Coatings Technology

journal homepage: www.elsevier.com/locate/surfcoat

Anti-corrosion characteristics of polyimide/h-boron nitride composite films with different polymer configurations

Yi-Chia Huang, Teng-Yuan Lo, Cheun-Guang Chao, Wha-Tzong Whang *

Department of Materials Science and Engineering, National Chiao Tung University, Taiwan

ARTICLE INFO

Available online 12 October 2014

Keywords:
Boron nitride
Polyimide
Anti-corrosion
Configuration
Crystallinity

ABSTRACT

Anti-corrosive polyimide/hexagonal boron nitride (PI/h-BN) composite films were prepared with different monomers to offer different polymer configurations: rigid and soft. In PI/h-BN composite films, different configurations of polymers show different crystallinity trends of the polymer matrix. In our study, the degree of crystallinity in rigid polymer decreases with the BN content; in flexible polymers it is independent of the BN content. It is worth noting that BN in different PI matrices can effectively enhance the protection of steel from corrosion. With a flexible PI matrix, the PI/h-BN coating exhibited better resistance to water vapor and better anti-corrosion. Only 5 wt.% of h-BN in the composite is enough to offer high anti-corrosion, a positive corrosion voltage.

1. Introduction

Polyimide (PI) shows good mechanical properties, such as low creep, low stress relaxation, high yield stress and high tensile strength [1–3]. Therefore, PI is a high performance polymer, lightweight, flexible, and resistant to heat, chemicals, and organic solvents [4–6]. Even though PI shows excellent chemical and thermal stability, water easily penetrates PI [5–7]. Water penetration reduces the protection of the PI coating barrier in anti-corrosion applications [8–10]. In order to decrease water penetration, many inorganic materials have been imported into the polymer matrix, such as silica [10,11], titanium oxide [12–14], clay [15–18] and graphene [19,20]. Generally, ceramic materials which are synthesized by the sol–gel method are spherical particles; however, spherical particles show worse barrier properties than 2-D flake materials in the polymer matrix on anti-corrosion applications. This is the reason why 2-D materials are widely used in anti-corrosion applications with polymer matrices [6,8,16–20].

Clay is a fine-grained soil that combines one or more clay minerals with traces of metal oxides. Usually, clay contains cations, which are quantified by the cation-exchange capacity (CEC). The CEC of clays used in anti-corrosion is about 100–120 meq/100 g [21–23]. Clay with high ion content in the polymer will enhance the ion conductivity of the anti-corrosive coating [23], which may reduce the stability and credibility of the anti-corrosion barrier, in turn, downgrading its anti-corrosion performance. A similar problem is also revealed in the graphene system. Graphene is an excellent electric conductor. Conductive graphene in the barrier layer may cause galvanic corrosion with other metals and/or reaction with another metal ion in the electrolyte. Boron nitride (BN) is a chemical compound with equal numbers of boron and nitrogen atoms. The hexagonal structure, as in graphene or carbon-related materials, is the most stable [24] packing of carbon atoms (belonging to group IV A). BN, compounds of boron and nitrogen atoms (groups III–V A), also have a stable hexagonal structure similar to graphene sheets. Because hexagonal boron nitride (h-BN) does not contain ions, it behaves as an excellent insulation. Therefore, we can expect that h-BN in a corrosion-protection coating may produce better anti-corrosion stability than clay and graphene. In addition, no previous study on BN in the polymer matrix has been reported for anti-corrosive applications. In this paper, we import h-BN to the PI matrix as a barrier layer, and evaluate its corrosion-protection characteristics with different PI matrices: rigid and soft. Dynamic mechanical analysis, X-ray diffraction (XRD), electrochemical measurements of Tafel plots, and the water vapor permeation test were undertaken to analyze the anti-corrosion related characteristics of the pristine PI matrix and the polyimide/hexagonal boron nitride (PI/h-BN) composite coating on steel.

2. Experimental

2.1. Materials

4,4′-Oxydianiline (ODA, 99.5%, Chriskev) and p-phenylenediamine (PDA, 99%, Aldrich) were vacuum-dried at 110 °C for 24 h prior to use. 3,3′,4,4′-Biphenyl tetracarboxylic dianhydride (BPDA, 99.5%, Chriskev) and 4,4′-(4,4′-isopropylidenediphenoxy)bis(phthalic anhydride) (IDPA, 97.5%, Chriskev) were purified by recrystallization using acetic anhydride (99.8%, Tedia). h-BN (Nanostructured and Amorphous Materials, Inc.) was vacuum-dried at 120 °C for 24 h to remove moisture. Molecular

* Corresponding author. Tel.: +886 3 5731873; fax: +886 3 5724727.
E-mail address: wtwhang@mail.nctu.edu.tw (W.-T. Whang).

http://dx.doi.org/10.1016/j.surfcoat.2014.09.043
0257-8972/

sieves (4 Å) were used to remove water from the solvent, N, N′-dimethylacetamide (DMAc, HPLC, Tedia).

2.2. Preparation of PI/h-BN composite films

The PI/h-BN composite films were synthesized using diamine (PDA, ODA), dianhydride (BPDA, IDPA) and h-BN. A stoichiometric amount of h-BN was dispersed in a given amount of DMAc with ultrasonication and mechanical stirring in a flask. Equimolars of diamine and dianhydride were slowly added to the above solution for polymerization. After all solid monomers had been dissolved in the solution the polymer precursor solution was kept at room temperature for 2 h. The resulting solution was cast on steel using a doctor blade and was then transformed into PI by chemical imidization at 150 °C for 1 h. The PI was synthesized by BPDA and PDA which is abridged to BP-PD; moreover, the PI is formed by IDPA and ODA named ID-OD. The chemical structures of BP-PD and ID-OD are shown in Scheme 1.

The pristine BPDA-PDA with symmetric configuration is a rigid polyimide and IDPA-ODA with kink configuration is a soft polyimide. The composite sample codes are denoted as BP-PD-x or ID-OD-x, where x represents the weight percentage of h-BN in each solid sample.

2.3. Measurements

A dynamic mechanical analyzer (DMA, TA Instruments, DMA 2980) was employed to determine the storage modulus (E′) and glass transition temperature (Tg) of pristine PI and composite films. Thermal gravimetric analysis (TGA, TA Instruments, Q500) was employed to determine the thermal stability of composite films. The crystalline characteristics were identified using XRD (Bruker, D2 Phaser). Electrochemical measurements of Tafel plots of coated steel 304 electrodes were taken with an electrochemical workstation (Jiehan 5600). The water vapor transmission rate (WVTR) of the composite films was measured with a permeation test system (Mocon, Permatran-W 3/61).

3. Results and discussion

The crystallinity difference between pristine PI and PI/h-BN composite films has been directly identified by XRD. Fig. 1 shows the XRD patterns of the symmetric-configuration BP-PD series and kink-configuration ID-OD series. The pristine BP-PD film in Fig. 1(a) exhibits two peaks of 2θ in the region of 12–26°, which identifies the pristine BP-PD a semi-crystalline polyimide, while the pristine ID-OD film in Fig. 1(b) displays a broad curve without peaks, which confirms that the ID-OD is an amorphous polymer. The symmetric configuration of the BP-PD shows a higher tendency for crystallization than the kink configuration of ID-OD. With h-BN in the BP-PD polyimide, the crystalline peak height of the matrix in Fig. 1(a) decreases with the h-BN weight fraction increasing. The higher h-BN fractions lead to lower peak heights

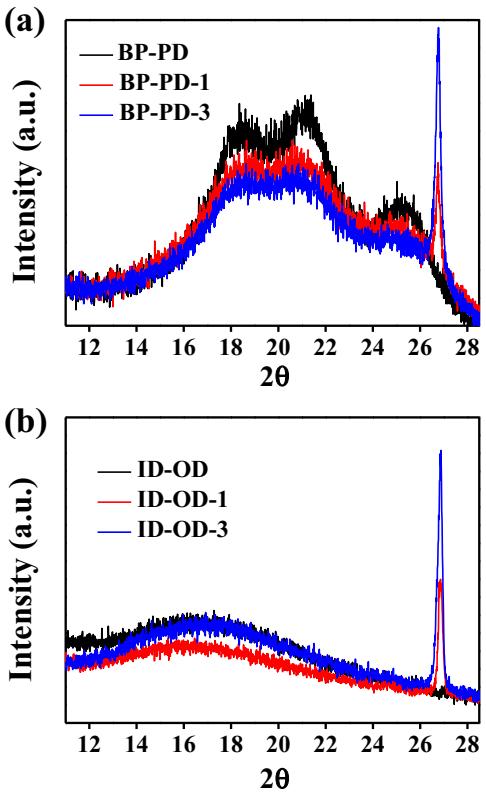

Fig. 1. XRD patterns of pristine PI and PI/h-BN composite films for (a) the BP-PD series and (b) the ID-OD series.

of the contributed PI, meaning that h-BN hinders the packing of rigid chains and in turn reduces the crystallization of the PI matrix. On the other hand, the XRD patterns of ID-OD-x films are similar to that of pristine ID-OD film, because the pristine PI is amorphous.

The storage moduli (E′) of PI and PI/h-BN composite films determined by DMA are displayed in Fig. 2. Because BP-PD is a semi-crystalline polymer and ID-OD an amorphous polymer, the former has a higher modulus than the latter. At temperatures no higher than 150 °C, both series of PI and PI-h-BN composites have the same trend of BN effects on the modulus. The modulus increases with the BN fraction. But there are differences in both series at higher temperatures. The rigid BP-PD and BP-PD-x in Fig. 2(a) keep their moduli above 1500 MPa below 250 °C while ID-OD and ID-OD-x downgrade their moduli at 220 °C. BP-PD shows higher modulus than BP-PD-1 and BP-PD-3, the reason is that BP-PD is a semi-crystal polymer, the modulus of crystal polymer should be higher than amorphous one. According to above reason, importing BN into BP-PD caused a reduction in polymer

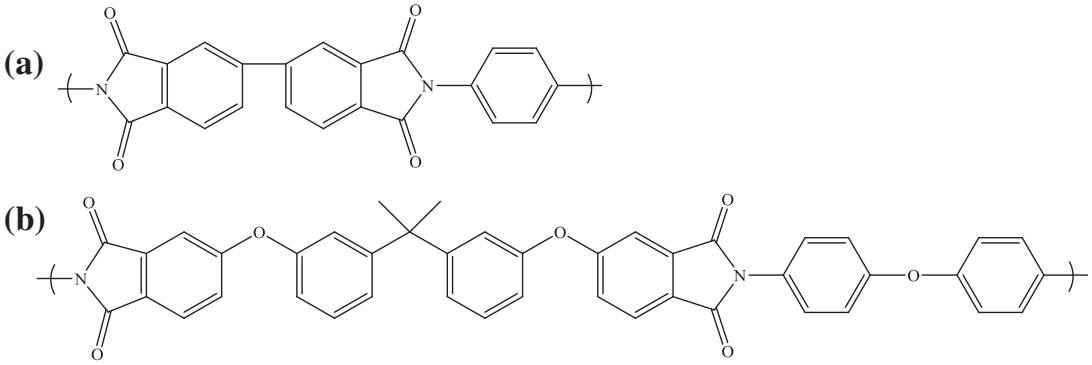

Scheme 1. The chemical structures of (a) BP-PD and (b) ID-OD.

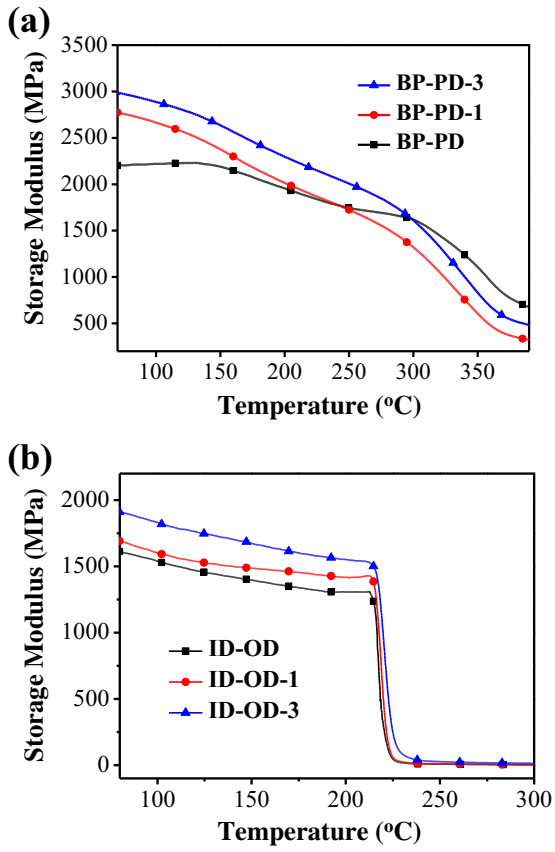

Fig. 2. The dynamic mechanical analysis of pristine PI and PI/h-BN composite films for (a) the BP-PD series and (b) the ID-OD series.

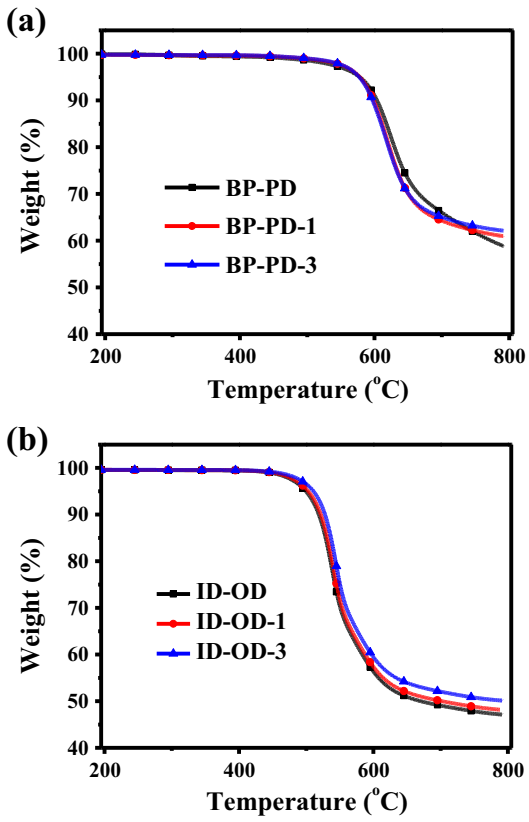

Fig. 3. The thermogravimetric curve of pristine PI and PI/h-BN composite films for (a) the BP-PD series and (b) the ID-OD series.

crystallinity. It means that the crystalline decreases with the increasing BN fraction in BP-PD series. It is the reason why BP-PD displays higher modulus than BP-PD-1 and BP-PD-3 at high temperature. In ID-OD series, the strength of modulus is no correlation with BN contents. The results are the same with XRD patterns. The TGA curves of composite film are shown in Fig. 3. In ID-OD series, thermal stability is promoted by increasing BN fractions, however, this trend is different from BP-PD series. In this case, thermal stability of polymer should relate to crystalline and filler fraction. Polymer displays better thermal stability with higher crystalline and more ceramic filler fraction. When BN is imported to BP-PD matrix, the crystalline of BP-PD decreased. The decreasing of crystalline should reduce thermal stability of BP-PD, the increasing of BN fraction should increase thermal stability of BP-PD. Base on the above reason, it is why the trend of BP-PD series is different from ID-OD series.

The advantages of the anti-corrosive application for h-BN compared with other 2D-flake materials in the polymer matrix are shown in Fig. 4. All these three types of polymer composites import 2D-inorganics as fillers; the fillers can increase the path length of the water and oxygen penetrating through the coated layer. The mechanism is used to improve the anti-corrosive characteristics. However, the fillers are different in electronic conductivity, ionic content and ionic conductivity. The h-BN displays excellent thermal conductivity; more importantly it is an outstanding insulator. It does not contain ions in the structure and therefore exhibits poor ionic conductivity. In the polymer/graphene coated layer, the electrons may tunnel or hop through graphene. Clay usually contains some ions which will increase ion content and ionic conductivity in the polymer composite layer. Electronic conductivity and ionic conductivity usually degrade the anti-corrosion properties. h-BN filler is an electric insulator with no ions, and is the best candidate for 2D fillers in anti-corrosion coated layers.

The anti-corrosion ability of PI/h-BN composite films was determined by the Tafel method. The Tafel plots of log I versus log E were acquired by scanning the potential range from −0.25 to +0.25 V, relative to the open circuit potential. Fig. 5 shows the Tafel plots of PI/h-BN composite films coated on steel 304; the coated samples exhibit a more positive corrosion potential than the raw steel. In the Tafel plots of the soft ID-OD series, the corrosion current density decreases with increasing BN content, and the corrosion potential becomes more positive with the increasing BN weight percentage. On the contrary, the rigid BP-PD series display a different trend in the changes in corrosion current density and corrosion potential. In Fig. 5(b), the sample with the

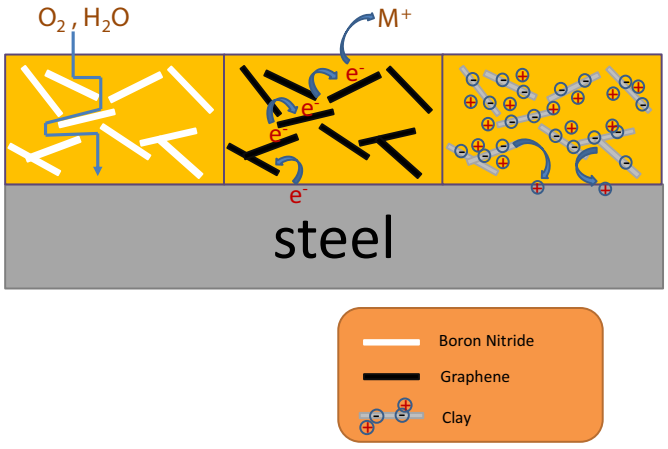

Fig. 4. The advantages of anti-corrosive application of h-BN compared with other 2D-flake materials in the polymer matrix.

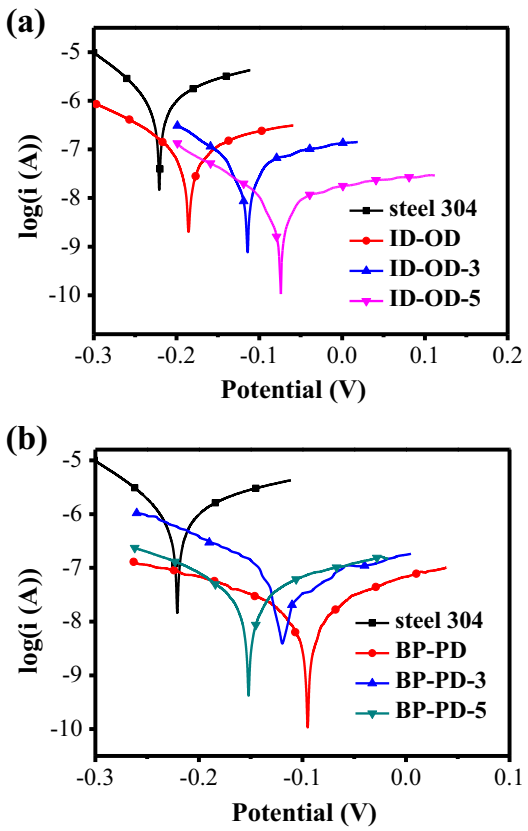

Fig. 5. The Tafel plots of pristine PI and PI/h-BN composites for (a) the ID-OD series and (b) the BP-PD series.

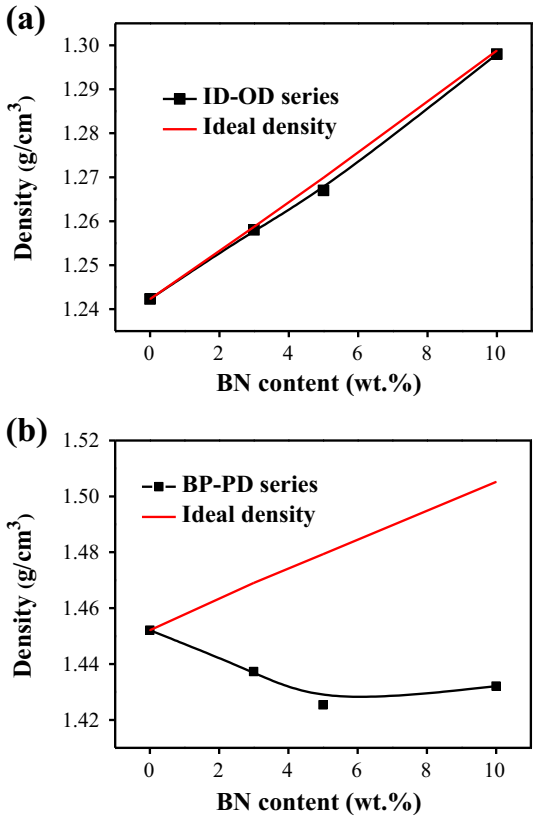

Fig. 6. Ideal densities and real densities of pristine PI and PI/h-BN composites for (a) the ID-OD series and (b) the BP-PD series.

pristine BP-PD coating shows the lowest corrosion current and most positive corrosion potential over the raw steel and BP-PD-3 and BP-PD-5 samples. The differences in crystallinity and thermal mechanical properties between the ID-OD series and the BP-PD series with various BN contents are shown in Figs. 1 and 2. Sugama and Gawlik reported that matrix crystallinity of the polymer composite might affect the anti-corrosion properties [25]. Generally, the polymer with the higher crystallinity coated on steel shows better barrier and anti-corrosion properties. In other words, the denser polymer exhibits better barrier properties than the loose [26]. Density measurement is a handy way to grasp the situation of polymer chain packing. The actual density and ideal density of PI/h-BN composite films are shown in Fig. 6 and Table 1. The ideal density (ρ) was calculated using the following equation: $\rho = (W_{PI} + W_{BN}) / (V_{PI} + V_{BN})$, where W_{PI} and W_{BN} are the weight of PI and BN in the composite films, and V_{PI} and V_{BN} are the volume of PI and BN. The ideal density and the actual density are very close in the ID-OD series. The actual densities are significantly lower than the ideal densities in the BP-PD series. In order to quantify the above polymer chain packing situation, fractional free volumes (FFVs) of PI matrix were calculated using the Bondi method [27]. As shown in Table 1, the FFVs of the PI matrix in the ID-OD series are close, independent of the h-BN content, but the FFVs in the BP-PD series increase with increasing h-BN content. Increasing FFV may cause easier water and oxygen penetration. The effect of h-BN content on the WVTR of the ID-OD and BP-PD series composite films is shown in Fig. 7. A continuous decrease in WVTR with increasing h-BN content is observed in the ID-OD series. An apparent decrease in WVTR by 84%, from 240 to 38 g m^{-2} day^{-1}, is achieved upon the addition of 5 wt.% of h-BN to the ID-OD. The BP-PD-x composite-coated samples have higher WVTR than the pristine BP-PD coated sample, quite different from the ID-OD series. This result is due to the crystallinity decreasing and the FFV increasing as h-BN is imported into the rigid BP-PD matrix.

4. Conclusions

We successfully prepared an excellent anti-corrosion PI/h-BN composite film by importing electric insulating 2D h-BN without ion content into the polyimides. Different configurations of the polyimide matrix (symmetric and kink) display different morphologies, semi-crystalline and amorphous. The polymer configuration in turn affects the barrier and anti-corrosion properties of the pristine PI-coated samples. It also affects the effect of the h-BN in the composites on these properties. The semi-crystalline BP-PD PI shows better stability at high temperature but poor anti-corrosion properties with h-BN importing. However, h-BN displays an excellent anti-corrosion barrier in the ID-OD amorphous polymer matrix, rather than in the pristine polymer matrix, and PI/h-BN composite films exhibited better resistance to water vapor than pure kink PI. Their performance enhances with BN content. With the addition of only 5 wt.% of h-BN in the kink PI, a significant reduction in the water vapor permeability rate by 84% was observed. The results suggest that by choosing the proper matrix, h-BN shows high potential in anti-corrosion applications.

Table 1
The density and FFV of BP-PD and ID-OD series composite films with various h-BN content.

Series	BN content (wt.%)	Density of composites (g/cm^3)	Density of PI* (g/cm^3)	FFV (%)
BP-PD	0	1.4521	1.4521	4.45
	3	1.4373	1.4223	6.41
	5	1.4254	1.3992	7.93
	10	1.4321	1.3786	9.29
IL-OD	0	1.2423	1.2423	19.97
	3	1.2580	1.2415	20.02
	5	1.2672	1.2395	20.15
	10	1.2981	1.2415	20.02

* The PI density with h-BN deduction.

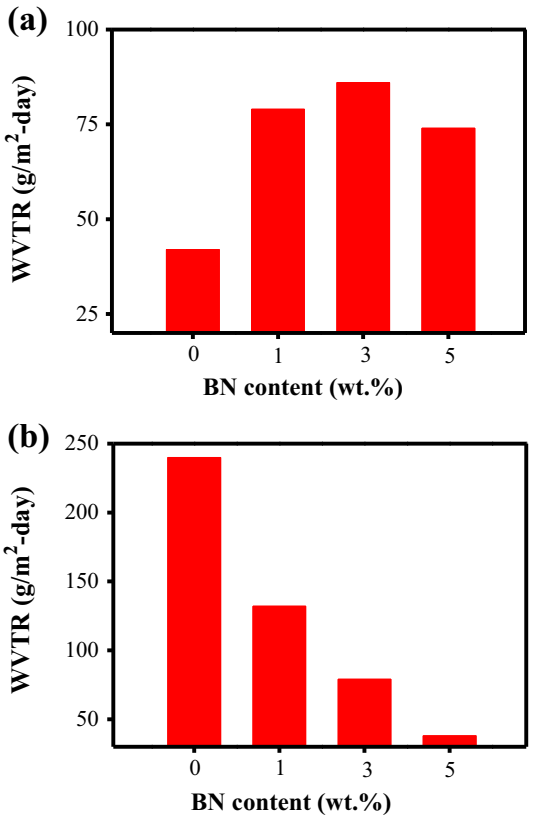

Fig. 7. WVTR of (a) the BP-PD series (b) the ID-OD series.

Acknowledgment

The authors would like to acknowledge the Ministry of Science and Technology of Taiwan (ROC) for the financial support through the project MOST 100-2221-E-009-023-MY3 and MOST 102-2221-E-009-175.

References

[1] Y. Nakamura, Y. Suzuki, Y. Watanabe, Thin Solid Films 290 (1996) 367–369.
[2] S.G. Hahm, S. Choi, S.H. Hong, T.J. Lee, S. Park, D.M. Kim, W.S. Kwon, K. Kim, O. Kim, M. Ree, Adv. Funct. Mater. 18 (2008) 3276–3282.
[3] P.-C. Chiang, W.-T. Whang, M.-H. Tsai, S.-C. Wu, Thin Solid Films 447 (2004) 359–364.
[4] M.-H. Tsai, Y.-C. Huang, I. Tseng, H.-P. Yu, Y.-K. Lin, S.-L. Huang, Thin Solid Films 519 (2011) 5238–5242.
[5] M.-H. Tsai, H.-Y. Wang, H.-T. Lu, I. Tseng, H.-H. Lu, S.-L. Huang, J.-M. Yeh, Thin Solid Films 519 (2011) 4969–4973.
[6] M.-H. Tsai, C.-J. Chang, H.-H. Lu, Y.-F. Liao, I. Tseng, Thin Solid Films 544 (2013) 324–330.
[7] C.R. Moylan, M.E. Best, M. Ree, J. Polym. Sci. B Polym. Phys. 29 (1991) 87–92.
[8] M. Bagherzadeh, F. Mahdavi, Prog. Org. Coat. 60 (2007) 117–120.
[9] A. Bouyanzer, B. Hammouti, Pigment Resin Technol. 33 (2004) 287–292.
[10] F. Zhang, S. Chen, L. Dong, Y. Lei, T. Liu, Y. Yin, Appl. Surf. Sci. 257 (2011) 2587–2591.
[11] D.J. Mills, S. Jamali, K. Paprocka, Surf. Coat. Technol. 209 (2012) 137–142.
[12] V. Karpakam, K. Kamaraj, S. Sathiyanarayanan, J. Electrochem. Soc. 158 (2011) C416–C423.
[13] G. Rajkumar, M.G. Sethuraman, Ind. Eng. Chem. Res. 52 (2013) 15057–15065.
[14] Z. Li, L. Ma, M. Gan, W. Qiu, D. Fu, S. Li, Y. Bai, Prog. Org. Coat. 76 (2013) 1161–1167.
[15] E. Faure, E. Halusiak, F. Farina, N. Giamblanco, C. Motte, M. Poelman, C. Archambeau, C.C. Van De Weerdt, J. Martial, C. Jérome, Langmuir 28 (2012) 2971–2978.
[16] M. Bagherzadeh, T. Mousavinejad, Prog. Org. Coat. 74 (2012) 589–595.
[17] M. Heidarian, M. Shishesaz, S. Kassiriha, M. Nematollahi, Prog. Org. Coat. 68 (2010) 180–188.
[18] F. Malin, B. Znoj, U. Šegedin, S. Skale, J. Golob, P. Venturini, Prog. Org. Coat. 76 (2013) 1471–1476.
[19] C.-H. Chang, T.-C. Huang, C.-W. Peng, T.-C. Yeh, H.-I. Lu, W.-I. Hung, C.-J. Weng, T.-I. Yang, J.-M. Yeh, Carbon 50 (2012) 5044–5051.
[20] K.-C. Chang, M.-H. Hsu, H.-I. Lu, M.-C. Lai, P.-J. Liu, C.-H. Hsu, W.-F. Ji, T.-L. Chuang, Y. Wei, J.-M. Yeh, Carbon 66 (2014) 144–153.
[21] C.-W. Chiu, T.-C. Lee, P.-D. Hong, J.-J. Lin, RSC Adv. 2 (2012) 8410–8415.
[22] T.-Y. Tsai, M.-J. Lin, Y.-C. Chuang, P.-C. Chou, Mater. Chem. Phys. 138 (2013) 230–237.
[23] R. Prasanth, N. Shubha, H.H. Hng, M. Srinivasan, Eur. Polym. J. 49 (2013) 307–318.
[24] R. Wentorf Jr., J. Chem. Phys. 34 (2004) 809–812.
[25] T. Sugama, K. Gawlik, Prog. Org. Coat. 42 (2001) 202–208.
[26] L. Li, Y. Yu, Q. Wu, G. Zhan, S. Li, Corros. Sci. 51 (2009) 3000–3006.
[27] D. Hofmann, M. Entrialgo-Castano, A. Lerbret, M. Heuchel, Y. Yampolskii, Macromolecules 36 (2003) 8528–8538.